



Tropical climate responses to projected Arctic and Antarctic sea-ice loss

Mark R. England^{1,2,3}✉, Lorenzo M. Polvani^{1,4}, Lantao Sun⁵ and Clara Deser⁶

Arctic and Antarctic sea-ice extent are both projected to dramatically decline over the coming century. The effects of Arctic sea-ice loss are not limited to the northern high latitudes, and reach deep into the tropics. Yet little is known about the effects of future Antarctic sea-ice loss outside of the southern high latitudes. Here, using a fully coupled climate model, we investigate the tropical response to Antarctic sea-ice loss and compare it with the response to Arctic sea-ice loss. We show that Antarctic sea-ice loss, similar to Arctic sea-ice loss, causes enhanced warming in the eastern equatorial Pacific and an equatorward intensification of the Intertropical Convergence Zone. We demonstrate that Antarctic sea-ice loss causes a mini global warming signal comparable to the one caused by Arctic sea-ice loss, and reminiscent of the response to greenhouse gases. We also show that ocean dynamics are key to capturing the tropical response to sea-ice loss. In short, we find that future Antarctic sea-ice loss will exert a profound influence on the tropics. Combined Arctic and Antarctic sea-ice losses will account for 20–30% of the projected tropical warming and precipitation changes under the high-emissions scenario Representative Concentration Pathway 8.5.

Over the past four decades, observed Arctic sea-ice extent (SIE) has dramatically decreased—September SIE has nearly halved since 1979¹, with an estimated 8,000 km³ of sea-ice volume lost over that period². At the other pole, Antarctic SIE has increased at a small, but significant, rate of 2% per decade over the period 1979–2015³. However, 2017 and 2018 set new records for minimum SIE in the Antarctic since satellite observations began in 1979¹, and a considerable decline in the sea-ice cover in both the Arctic and Antarctic is expected by the end of this century⁴. Under the high-emissions scenario, models predict that the first ice-free Arctic summer will occur by the middle of this century^{5–7}, and Antarctica may lose one-half of its sea-ice cover by 2100⁴. To understand the full effect of these dramatic changes on the climate system, here we study the impact of future Arctic and Antarctic sea-ice losses, both separately and together.

The high-latitude response to Arctic sea-ice loss is well established, and involves an intense warming and moistening of the polar atmosphere^{8–10}, especially near the surface. The mounting body of modelling work on Arctic sea-ice loss indicates that likely impacts also include a weakening and equatorward shift of the tropospheric jet^{11–15} and a slowdown in the Atlantic Meridional Overturning Circulation^{16–19}. When sea-ice perturbations are imposed in an atmosphere-only model configuration, the effects are confined to the mid- and high latitudes^{12,20}. However, in the presence of ocean dynamics, sea-ice loss can have global effects^{16,20–22} with important impacts that extend to the tropics^{18,22–24}.

In contrast to the flurry of activity to understand the impacts of sea-ice loss in the Arctic, work on the impacts of projected Antarctic sea-ice loss is only now starting. So far, just four studies have investigated the effects of projected Antarctic sea-ice loss; three were based on atmosphere-only models^{12,25,26} and the fourth inferred the response from the Coupled Model Intercomparison Project Phase 5 (CMIP5) archive²⁷. However, due to the lack of ocean dynamics,

these modelling studies have probably not captured the full extent of the global response. Our study addresses this by examining the tropical effects of Antarctic sea-ice loss using a fully coupled model that includes ocean dynamics.

Arctic sea-ice loss has been shown to impact tropical sea surface temperatures (SSTs), the position of the Intertropical Convergence Zone (ITCZ) and the strength and location of the Hadley Cell^{16,18,21–24,28}. Zonal asymmetries in the tropical SST response are linked to ocean dynamics, with enhanced warming in the eastern equatorial Pacific^{16,18,19,21–23}. This response is accompanied by an increase in rainfall over the equatorial Pacific, roughly symmetric about the Equator, which intensifies at the equatorward edge of the ITCZ^{16,18,21–23}.

But how do the tropics respond to Antarctic sea-ice loss? This is the key question of this study. We answer it with a fully coupled (that is, with interactive sea-ice and ocean components) global climate model, CESM-WACCM²⁹. In brief, we specify projected sea-ice loss at the end of this century using the ‘ghost flux’ method²¹, and we contrast the climate in long time-slice integrations with projected loss in the Arctic (hereafter A), the Antarctic (hereafter AA) and both (hereafter A&AA) to the climate of a control run: the difference is the response to sea-ice loss. We address four questions with these runs: (1) will future AA sea-ice loss have an important impact on the tropics?; if so, (2) how does the tropical response to AA sea-ice loss compare, in pattern and in magnitude, with the tropical response to A sea-ice loss?; (3) are the responses to A and AA sea-ice loss linearly additive?; and (4) taken together, how much of the Representative Concentration Pathway 8.5 (RCP8.5) response is attributable to the combined effects of A and AA sea-ice loss?

The tropical response to A and AA sea-ice loss

The latitude–height structure of the zonal-mean atmospheric temperature responses to A and AA sea-ice loss exhibit strong

¹Department of Applied Physics and Applied Mathematics, Columbia University, New York, NY, USA. ²Department of Physics and Physical Oceanography, University of North Carolina Wilmington, Wilmington, NC, USA. ³Department of Climate, Atmospheric Science, and Physical Oceanography, Scripps Institution of Oceanography, UCSD, La Jolla, CA, USA. ⁴Department of Earth and Environmental Science, Lamont Doherty Earth Observatory, Columbia University, New York, NY, USA. ⁵Department of Atmospheric Science, Colorado State University, Fort Collins, CO, USA. ⁶National Center for Atmospheric Research, Boulder, CO, USA. ✉e-mail: mengland@ucsd.edu

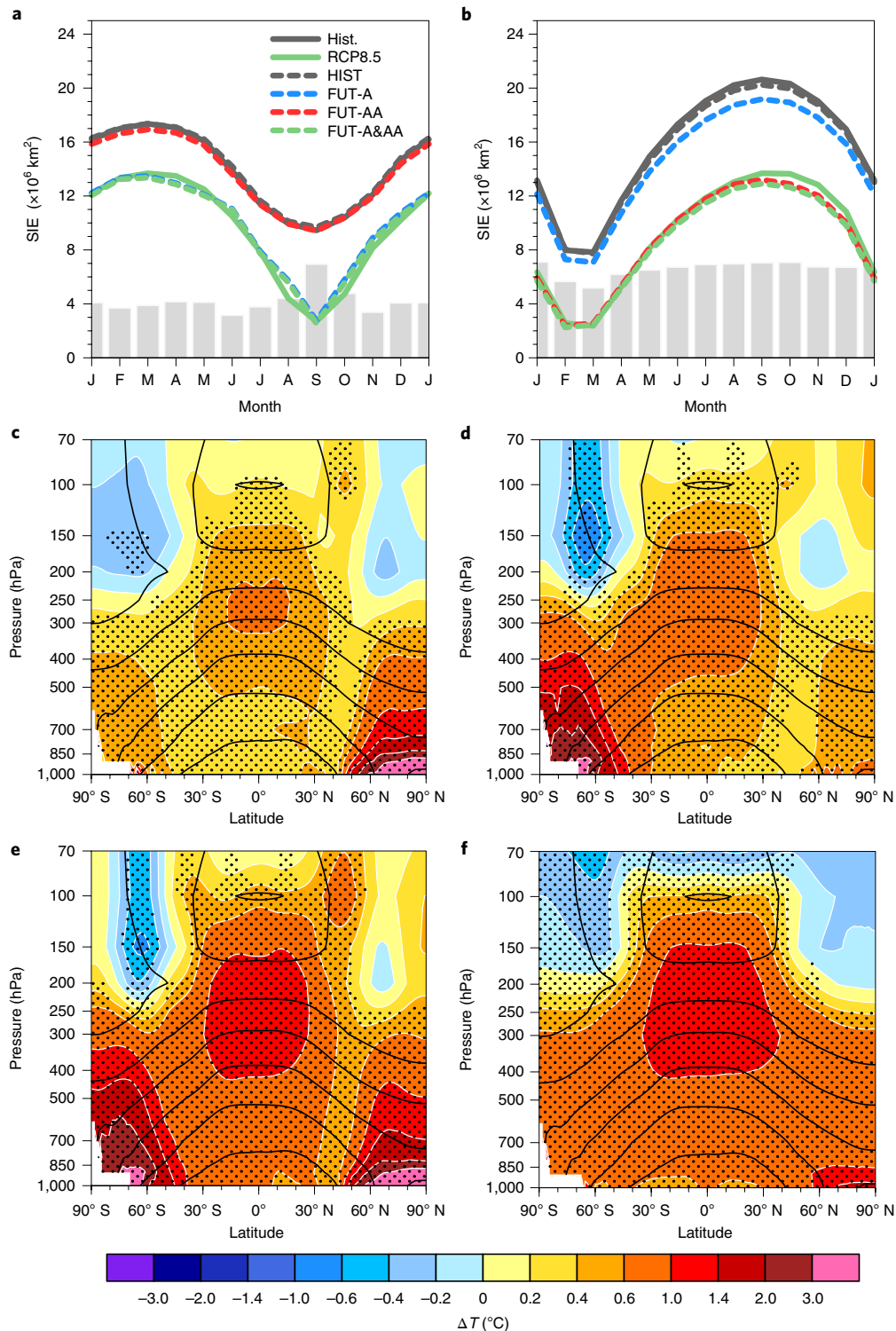


Fig. 1 | Seasonal cycle of SIE in experiments and the zonally averaged temperature response to sea-ice loss. **a, b**, The seasonal cycle of A (**a**) and AA (**b**) SIE in the four experiments (dashed lines: HIST, FUT-A, FUT-AA and FUT-A&AA). The solid lines show the target SIE values from the historic runs averaged over 1955–1969, and the RCP8.5 runs averaged over 2085–2099. The grey bars indicate the magnitude of the reduction in SIE between the HIST and FUT experiments. **c–e**, Zonally averaged atmospheric temperature response (ΔT) as a function of latitude and height to A (**c**), AA (**d**) and A&AA (**e**) sea-ice losses. **f**, RCP8.5 ΔT (the 15-yr average of 2085–2099 minus the 15-yr average of 1955–1969, averaged from six WACCM historical and three RCP8.5 runs) scaled by a factor of 1/5 to match the tropical upper tropospheric warming from **e**. Stippling indicates that the response is significant at the 95% confidence level using a two-sided Student's *t*-test.

similarities (Fig. 1c,d). In particular, both feature significant warming throughout the global troposphere, with maximum amplitude at high latitudes below 700hPa in the ice-loss hemisphere and a

secondary maximum in the upper tropical troposphere. This response resembles the structure of the full climate response to RCP8.5 (Fig. 1f), but with reduced amplitude, hence the term ‘mini

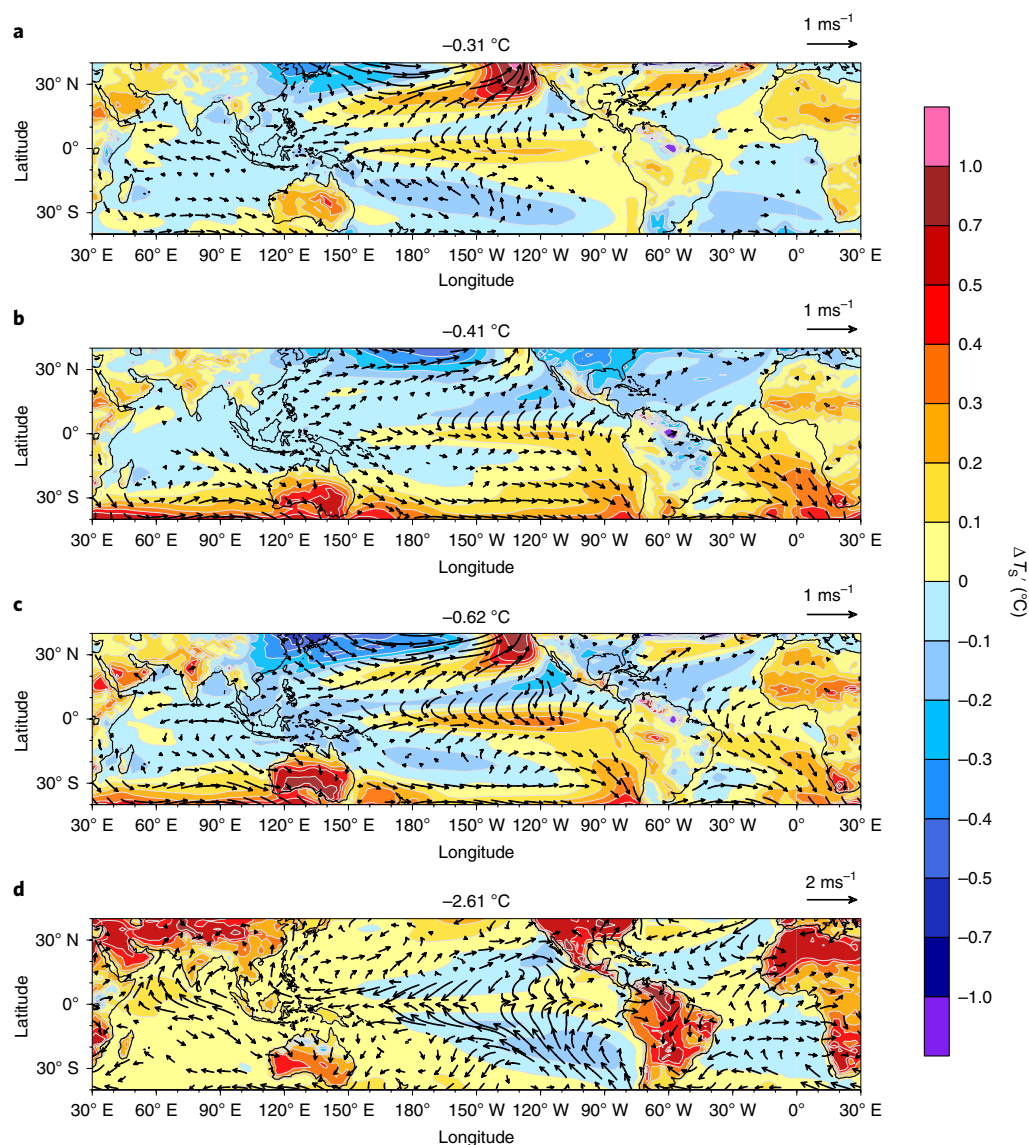


Fig. 2 | The tropical surface temperature (with tropical mean removed) and surface wind response to sea-ice loss. a–d, The patterns of annual mean surface temperature (T_s) response (colour scale) to A (a), AA (b) and A&AA (c) sea-ice losses and the projected changes under RCP8.5 (d), which are given by the 2085–2099 average minus the 1955–1969 average (scaled by a factor of 1/5). The tropical mean SST warming, shown above the maps, has been subtracted from each panel to emphasize the pattern of the response. See Extended Data Fig. 3 for the T_s response without the tropical mean removed. Vectors show the annual mean surface wind response. Note that while $\Delta T_s'$ under RCP8.5 has been scaled by 1/5, the surface wind vectors for the same panel have been scaled by a factor of 1/2 for clarity (the ' symbol indicates the anomaly from the tropical mean).

global warming' used in previous studies^{10,21,30,31}. When both A and AA sea-ice loss are imposed simultaneously (Fig. 1e), the increase in tropical upper tropospheric temperature is 1–1.5 °C, which accounts for approximately 20% of the warming under RCP8.5 in the tropical upper troposphere (Fig. 1f). The response to A sea-ice loss and AA sea-ice loss are approximately additive (panels c + d \approx e in Fig. 1), although the sum of the individual responses (A + AA) overestimates the combined (A&AA) response by 10–15% (Extended Data Fig. 2).

The surface temperature responses to sea-ice loss are shown in Extended Data Fig. 3 for the domain 40°N–40°S. Both A and AA sea-ice loss cause warming throughout the global tropics and subtropics, with maximum amplitudes (\sim 0.5 °C) along the equatorial Pacific cold tongue (Extended Data Fig. 3a,b). To highlight the pattern of the surface temperature response to polar sea-ice loss, in Fig. 2 we remove the tropical mean (20°S–20°N) response (0.31 °C for A, 0.41 °C for AA, 0.62 °C for A&AA and 2.61 °C for RCP8.5).

The equatorial warming maximum is accompanied by enhanced warming in the northeast subtropical Pacific in the case of A sea-ice loss (Fig. 2a), and in the southeast subtropical Pacific in the case of AA sea-ice loss (Fig. 2b), reminiscent of the structures of the Pacific Meridional Modes^{32–35}. In addition, AA sea-ice loss produces enhanced surface warming over the subtropical southeast Atlantic and the southern Indian Ocean (Fig. 2b). The surface temperature response to A&AA sea-ice loss (Fig. 2c and Extended Data Fig. 3c) combines all of these features in a linear fashion with warming in the northeast and southeast subtropical Pacific and equatorial Pacific. The pattern correlation between the response to A&AA sea-ice loss and the sum of the individual responses A + AA (Extended Data Fig. 4) is 0.82 for the region 30°S–30°N. The pattern of the surface temperature response to AA sea-ice loss is consistent with the results of the Extratropical-Tropical Intercomparison Model Comparison Project³⁶.

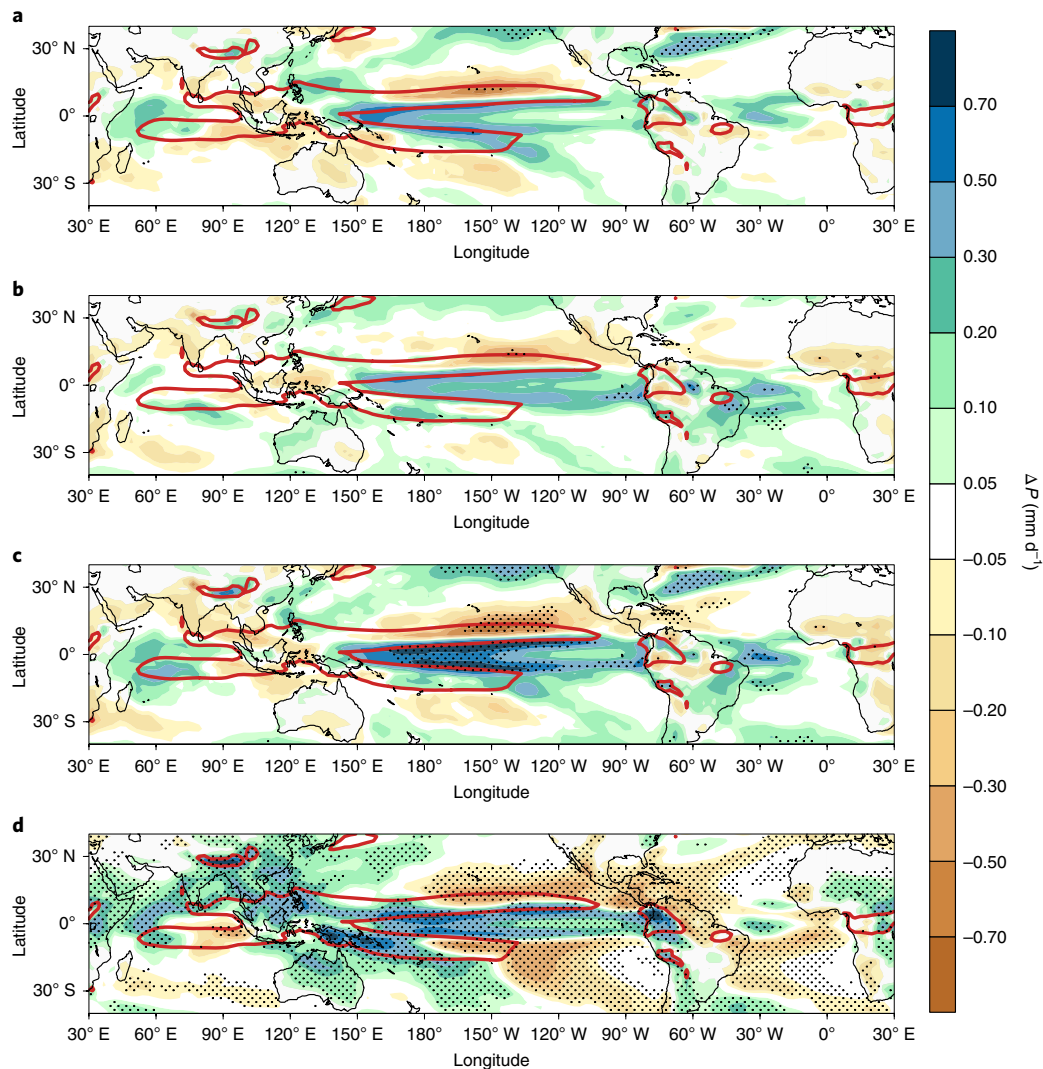


Fig. 3 | The tropical precipitation response to sea-ice loss. a–d. The annual mean precipitation response (ΔP) to A (a), AA (b) and A&AA (c) sea-ice loss and the projected changes under RCP8.5 (d), which are given by 2085–2099 average minus the 1955–1969 average (scaled by a factor of 1/3). The red contour shows the 6 mm d^{-1} precipitation climatology. Stippling indicates that the response is significant at the 95% confidence level using a two-sided Student's *t*-test.

Overall, the tropical mean surface warming response to the combined A&AA sea-ice loss accounts for 24% of the tropical mean SST change under RCP8.5 (0.62°C and 2.61°C respectively). However, we stress some important differences between the warming patterns associated with sea-ice loss and those projected under RCP8.5. Firstly, the RCP8.5 response contains less regional structure in the tropics (Fig. 2d and Extended Data Fig. 3d). In particular, the enhanced warming in the eastern equatorial Pacific relative to the western equatorial Pacific in response to sea-ice loss is largely absent in the RCP8.5 response. Furthermore, in contrast to the response to AA sea-ice loss (Fig. 2b), the RCP8.5 projection (Fig. 2d) exhibits a reduced warming in the southeast subtropical Pacific and Atlantic relative to the rest of the tropics.

As seen from the overlaid vectors in Fig. 2, both A and AA sea-ice losses lead to anomalous westerly winds in the equatorial Pacific, which act to weaken equatorial ocean upwelling. The surface wind response also features anomalous convergence in regions of enhanced SST warming, namely the northeast subtropical Pacific in the case of A sea-ice loss (Fig. 2a), the southeast subtropical Pacific and Atlantic in the case of AA sea-ice loss (Fig. 2b) and the eastern equatorial Pacific in the case of sea-ice loss from either pole.

The RCP8.5 response exhibits similar convergence in the eastern equatorial Pacific; however, in the southern subtropics the RCP8.5 response includes anomalous easterly winds in the western equatorial Pacific and anomalous divergence in the southeast subtropical Pacific, which are opposite in sign to the response to A&AA sea-ice losses. Thus, many of the effects of AA sea-ice loss act to oppose the full RCP8.5 projection (compare the vectors in Fig. 2b,d). Overall, sea-ice loss in either hemisphere results in a weakening of the wind-driven tropical cells and an enhanced warming of equatorial Pacific SSTs.

Next, we show that A and AA sea-ice losses produce remarkably similar amplitudes and patterns of tropical precipitation response (Fig. 3a,b). The uncentred pattern correlation between the precipitation response to A sea-ice loss and the response to AA sea-ice loss is 0.69 in the tropics (20°S – 20°N), and 0.79 in the tropical Pacific (20°S – 20°N , 130°E – 100°W). In particular, sea-ice loss at either pole causes an increase in precipitation on the equatorward edges of the Pacific ITCZs, and a reduction south of Hawaii on the poleward flank of the northern ITCZ. A&AA sea-ice loss (Fig. 3c) leads to an increase in precipitation of nearly 0.3 mm day^{-1} over the equatorial Pacific, and a decrease of 0.2 mm day^{-1} south of Hawaii.

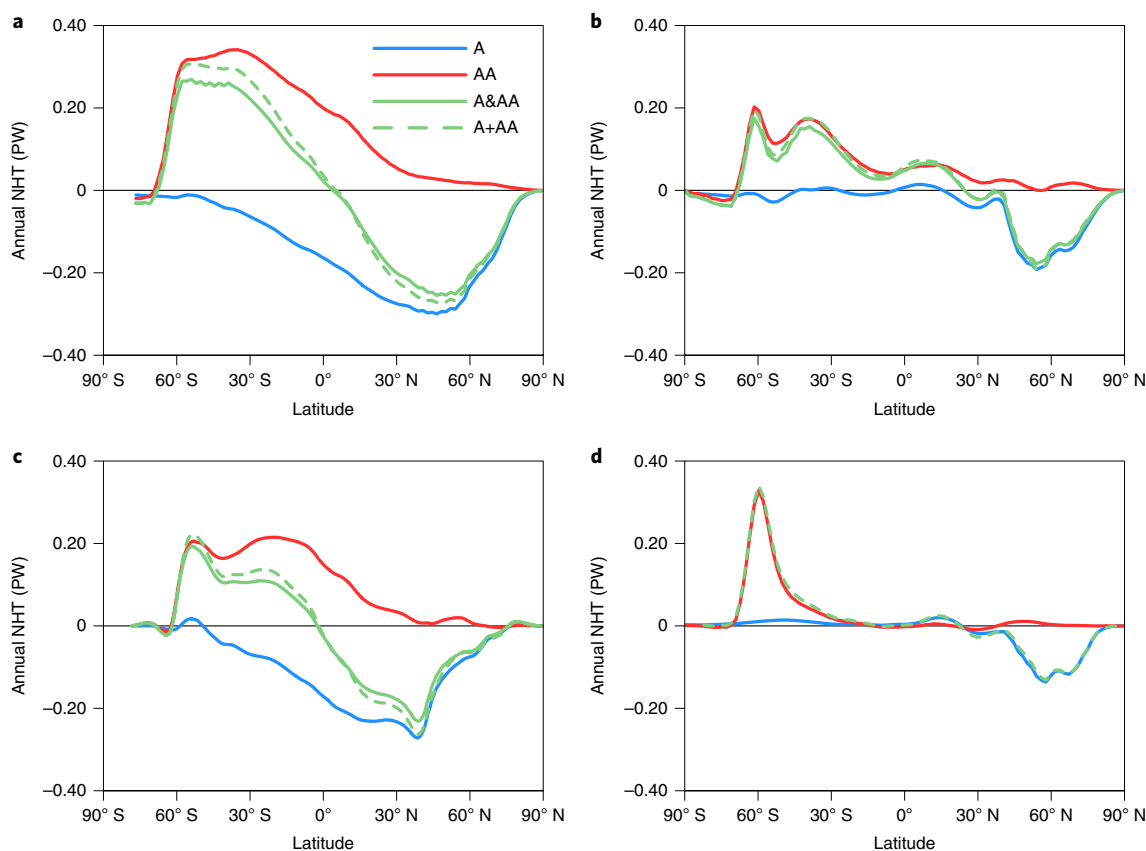


Fig. 4 | The response of northward atmospheric and oceanic heat transport to sea-ice loss. a–c, The average annual response of NHT to A, AA, A&AA and A+AA (the sum of the response to A and AA) sea-ice losses in the atmosphere+ocean (**a**), atmosphere (**b**) and ocean (**c**). **d**, The atmospheric NHT responses from the uncoupled simulations of England et al.¹².

The equatorial precipitation response to sea-ice loss is associated with an intensification of the heating maxima near the Equator in the mid- and upper troposphere (Extended Data Fig. 5), consistent with results from Deser et al.²¹. Similarly, the reduced precipitation over the Pacific at 10°N in response to sea-ice loss in either hemisphere (Fig. 3a,b) is consistent with the reduction in the condensational heating rate at this latitude (Extended Data Fig. 5). The pattern of precipitation response to A&AA sea-ice loss is similar to the RCP8.5 response (Fig. 3d), but with approximately one-third of the amplitude. However, the reduced precipitation over much of the southeastern tropical Pacific and a branch of enhanced precipitation further west are features found only in the RCP8.5 projection.

Confirming the results previously reported for the A sea-ice loss response²¹, the changes in tropical precipitation in our experiments (Fig. 3) can be understood using the pattern of the local SST response (Fig. 2 and Extended Data Fig. 3), which is in turn determined by ocean dynamics. Reduced equatorial upwelling leads to enhanced warming in the equatorial Pacific. The effects of rotation are negligible, thus pressure gradients are needed to balance the temperature gradients, and the resultant surface wind pattern produces anomalous convergence (Fig. 2, vectors), and hence increased precipitation, at the Equator.

The equatorial enhancement of zonal-mean precipitation in response to polar sea-ice loss migrates seasonally with the mean precipitation maxima (see Extended Data Fig. 6 for the zonal average and Extended Data Fig. 7 for the Pacific-sector average). In particular, positive precipitation anomalies occur around 5°N during boreal summer and around 5–10°S during boreal winter, following the equatorward edge of the dominant ITCZ in each season. The months in which the tropical precipitation response to A&AA

sea-ice loss is highest (December and January) are also the months in which the RCP8.5 projected response is weakest. Indeed, during these months, sea-ice loss accounts for half of the RCP8.5 response (Extended Data Fig. 6 and Extended Data Fig. 7).

Connecting sea-ice loss to the tropics

We now elucidate the mechanism that allows polar sea-ice loss to affect the tropics. From an energetic perspective, the response of the coupled atmosphere–ocean system to polar sea-ice loss consists of a change in northward heat transport (NHT) needed to offset the hemispheric radiative imbalance induced by the imposed sea-ice loss. The response of the NHT reaches into the tropics, and even into the opposite hemisphere (Fig. 4a). Although the partitioning between the atmospheric (Fig. 4b) and oceanic (Fig. 4c) contributions is different in response to A and AA sea-ice loss, the latitudinal structure of the total NHT response (Fig. 4a) is broadly similar (but reversed in sign and latitude). This leads to a response of NHT to A&AA sea-ice loss that is antisymmetric about the Equator and thus converges heat into the tropics. In the absence of atmosphere–ocean coupling and ocean heat transport (Fig. 4d), the response to sea-ice loss is confined to the mid- and high latitudes^{12,20,21}.

The tropical response to A sea-ice loss (blue curves in Fig. 4) is entirely due to oceanic heat transport (Fig. 4c) because the atmospheric heat transport vanishes south of 30°N (Fig. 4b). In contrast, the tropical response to AA sea-ice loss (red curves in Fig. 4) is mediated by NHT in both the atmosphere and the ocean (Fig. 4b,c), although with a larger oceanic contribution. Another interesting contrast is that coupling the atmosphere to a dynamic ocean slightly strengthens the mid-latitude atmospheric NHT response to A sea-ice loss (from a peak of –0.13 PW to –0.18 PW near 50°N;

Fig. 4b,d), but considerably weakens the mid-latitude atmospheric NHT response to AA sea-ice loss (from a peak of 0.35 PW to 0.22 PW near 60°S; Fig. 4b,d). This asymmetry is probably due to the dominant role of the Southern Ocean at southern mid-latitudes.

As reported in previous studies^{16,23}, we find that the tropical response to polar sea-ice loss is largely mediated by a slowdown of the oceanic subtropical meridional overturning cells (Extended Data Fig. 8), primarily in the ice-loss hemisphere. The slowdown of these subtropical cells reduces the upwelling of cold water at the Equator and the transport of heat away from the deep tropics, resulting in the enhanced equatorial surface warming²³. But how is the slowdown of the subtropical cells linked to the loss of polar sea ice? Here we focus on the case of AA sea-ice loss. First, we note that the subduction branches of the subtropical cells have a non-zonal spatial structure³⁷ (areas enclosed by the white contours in Extended Data Fig. 9a). In response to AA sea-ice loss, three distinct lows of sea-level pressure develop over the Southern Ocean (Extended Data Fig. 9b), with accompanying cyclonic winds (vectors in Extended Data Fig. 9b), consistent with results from ref. 22. These northwesterly winds over the subduction zones drive Ekman suction (red colours in Extended Data Fig. 9c), thereby reducing the downwelling in the subtropics and hence weakening the subtropical cell³⁸ (Extended Data Fig. 8b). The causal link between AA sea-ice loss and the northwesterly wind response in the subtropics originates in the atmosphere, as shown by the atmosphere-only experiment (Extended Data Fig. 9d), but ocean–atmosphere interactions enhance the magnitude of the wind response and extend its reach into lower latitudes (Extended Data Fig. 9b). We calculate the average Ekman suction response for the three subduction zones (Indian, Pacific and Atlantic) (white bars in Extended Data Fig. 10) and find it to be in good agreement with the vertical velocity response in these regions (black bars in Extended Data Fig. 10). The Ekman-driven upwelling response ($w_{\text{ek}} \approx 0.5 \text{ cm yr}^{-1}$) corresponds to a 5–10% reduction in downwelling (see Extended Data Fig. 9a) and is comparable in amplitude to the weakening of the subtropical cell (Extended Data Fig. 8b). Whether this precise mechanism is robust across other models remains to be determined.

Polar sea-ice loss and tropical climate change

To summarize, we return to the four questions that we posed at the start. Our experiments indicate that (1) projected AA sea-ice loss will have an important impact on the tropics, causing a warming in the upper troposphere, enhanced surface warming in the eastern Pacific and increased precipitation over the Pacific ITCZ region. (2) The tropical responses to end-of-century A and AA sea-ice losses are similar in both magnitude and spatial patterns, especially in the deep tropics. (3) The responses to A and AA sea-ice losses are approximately additive, although overestimate the combined response by 10–15%. (4) Together, projected A and AA sea-ice losses account for between one-fifth and one-third of the full response to RCP8.5 radiative forcing. Our results will need to be confirmed with other fully coupled climate models, especially for the Southern Ocean response. However, the tropical response to A sea-ice loss in our runs is very similar to that found in the GFDL-CM3¹⁸ and CCSM4^{16,21–23} models, lending support to our results.

In the case of A sea-ice loss, a fully dynamic ocean is needed to capture the regional pattern of tropical warming^{16,21,23}. As in our experiments, Wang et al.²³ determined that the enhanced equatorial Pacific warming in response to A sea-ice loss is largely caused by subsurface ocean warming, which itself was driven by reduced equatorial upwelling. We note, in addition, that the surface temperature response to AA sea-ice loss found in this study resembles the pattern that Hwang et al.³⁹ found when investigating the effect of increased Southern Ocean heat uptake, but with the opposite sign. Their model used a slab ocean configuration, and thus did not include the effect of ocean circulation (which our study suggests

is important for capturing the tropical response). Hwang et al.³⁹ argued that the wind–evaporation–SST feedback mechanism may be responsible for the tropical warming pattern, but we find little evidence for this mechanism in our experiment.

The tropics have long been known to have an important influence on the mid- and high-latitude climate^{40,41}. Chiang and Bitz²⁸ presented an early example of influence in the opposite direction, and showed how the polar regions can substantially affect the low latitudes. Our results provide further evidence for this mechanism and clearly indicate that, over the coming century, both the Arctic and the Antarctic will exert a profound influence on the tropics due to projected sea-ice losses.

Online content

Any methods, additional references, Nature Research reporting summaries, source data, extended data, supplementary information, acknowledgements, peer review information; details of author contributions and competing interests; and statements of data and code availability are available at <https://doi.org/10.1038/s41561-020-0546-9>.

Received: 14 September 2019; Accepted: 30 January 2020;

Published online: 16 March 2020

References

1. *All About Sea Ice* (National Snow and Ice Data Center, 2019); https://nsidc.org/data/seaice_index/
2. Schweiger, A. et al. Uncertainty in modelled Arctic sea ice volume. *J. Geophys. Res. Oceans* **116**, C00D06 (2011).
3. Comiso, J. et al. Positive trend in the Antarctic sea ice cover and associated changes in surface temperature. *J. Clim.* **30**, 2251–2267 (2017).
4. Collins, M. et al. in *Climate Change 2013: The Physical Science Basis* (eds Stocker, T. F. et al.) Ch. 12 (IPCC, Cambridge Univ. Press, 2013).
5. Liu, J., Song, M., Horton, R. & Hu, Y. Reducing spread in climate model projections of a September ice free Arctic. *Proc. Natl Acad. Sci. USA* **110**, 12571–12576 (2013).
6. Overland, J. & Wang, M. When will the summer Arctic be nearly sea ice free? *Geophys. Res. Lett.* **40**, 2097–2101 (2013).
7. Jahn, A., Kay, J., Holland, M. & Hall, D. How predictable is the timing of a summer ice-free Arctic? *Geophys. Res. Lett.* **43**, 9113–9120 (2016).
8. Liu, J., Curry, J., Wang, H., Song, M. & Horton, R. Impact of declining Arctic sea ice on winter snowfall. *Proc. Natl Acad. Sci. USA* **109**, 4074–4079 (2012).
9. Deser, C., Tomas, R., Alexander, M. & Lawrence, D. The seasonal atmospheric response to projected Arctic sea ice loss in the late twenty-first century. *J. Clim.* **23**, 333–351 (2010).
10. Screen, J. et al. Consistency and discrepancy in the atmospheric response to Arctic sea ice loss across climate models. *Nat. Geosci.* **11**, 155–163 (2018).
11. Screen, J. & Blackport, R. How robust is the atmospheric response to projected Arctic sea ice loss across Climate models? *Geophys. Res. Lett.* **46**, 11406–11415 (2019).
12. England, M., Polvani, L. & Sun, L. Contrasting the Antarctic and Arctic atmospheric responses to projected sea ice loss in the late twenty-first century. *J. Clim.* **31**, 6353–6370 (2018).
13. Screen, J., Simmonds, I., Deser, C. & Tomas, R. The atmospheric response to three decades of observed Arctic sea ice loss. *J. Clim.* **26**, 1230–1248 (2013).
14. Peings, Y. & Magnusdottir, G. Response of the wintertime northern hemisphere atmospheric circulation to current and projected Arctic sea ice decline. *J. Clim.* **27**, 244–264 (2014).
15. Sun, L., Deser, C. & Tomas, R. Mechanisms of stratospheric and tropospheric circulation response to projected Arctic sea ice loss. *J. Clim.* **28**, 7824–2845 (2015).
16. Tomas, R., Deser & Sun, L. The role of ocean heat transport in the global climate response to projected Arctic sea ice loss. *J. Clim.* **29**, 6841–6859 (2016).
17. Sevellec, F., Fedorov, A. & Liu, W. Arctic sea ice decline weakens the Atlantic Meridional Overturning Circulation. *Nat. Clim. Change* **7**, 604–610 (2017).
18. Sun, L., Alexander, M. & Deser, C. Evolution of the global coupled climate response to Arctic sea ice loss during 1990–2090 and its contribution to climate change. *J. Clim.* **31**, 7823–7843 (2018).
19. Liu, W. & Fedorov, A. Global impacts of Arctic sea ice loss mediated by the Atlantic Meridional Overturning Circulation. *Geophys. Res. Lett.* **46**, 944–952 (2019).
20. Smith, D. et al. Atmospheric response to Arctic and Antarctic sea ice: the importance of ocean–atmosphere coupling and the background state. *J. Clim.* **30**, 4547–4565 (2017).

21. Deser, C., Tomas, R. & Sun, L. The role of ocean-atmosphere coupling in the zonal-mean atmospheric response to Arctic sea ice loss. *J. Clim.* **28**, 2168–2186 (2015).
22. Sun, L., Deser, C., Tomas, R. & Alexander, M. Global coupled climate response to polar sea ice loss: evaluating the effectiveness of different ice-constraining approaches. *Geophys. Res. Lett.* **47**, e2019GL085788 (2020).
23. Wang, K., Deser, C., Sun, L. & Tomas, R. Fast response of the tropics to an abrupt loss of Arctic sea ice via ocean dynamics. *Geophys. Res. Lett.* **45**, 4264–4272 (2018).
24. Chemke, R., Polvani, L. & Deser, C. The effect of Arctic sea ice loss on the Hadley circulation. *Geophys. Res. Lett.* **46**, 963–972 (2019).
25. Kidston, J., Taschetto, A., Thompson, D. & England, M. The influence of Southern Hemisphere sea ice extent on the latitude of the mid-latitude jet stream. *Geophys. Res. Lett.* **38**, L15804 (2011).
26. Bader, J., Flugge, M., Kyamsto, N., Mesquita, M. & Voigt, A. Atmospheric winter response to a projected future Antarctic sea ice reduction: a dynamical analysis. *Clim. Dynam.* **40**, 2707–2718 (2013).
27. Ayres, H. & Screen, J. Multi-model analysis of the atmospheric response to Antarctic sea ice loss at quadrupled CO₂. *Geophys. Res. Lett.* **46**, 9861–9869 (2019).
28. Chiang, J. & Bitz, C. Influence of high latitude ice cover on the marine Intertropical Convergence Zone. *Clim. Dynam.* **25**, 477–496 (2005).
29. Marsh, D. et al. Climate change from 1850 to 2005 simulated in CESM1(WACCM). *J. Clim.* **26**, 7372–7391 (2013).
30. Blackport, R. & Kushner, P. The transient and equilibrium climate response to rapid summertime sea ice loss in CCSM4. *J. Clim.* **29**, 401–417 (2016).
31. Oudar, T. et al. Respective roles of direct GHG radiative forcing and induced Arctic sea ice loss on the Northern Hemisphere atmospheric circulation. *Clim. Dynam.* **49**, 3693–3717 (2017).
32. Chiang, J. & Vimont, D. Analogous Pacific and Atlantic meridional modes of tropical atmosphere–ocean variability. *J. Clim.* **17**, 4143–4158 (2004).
33. Amaya, D. The Pacific Meridional Mode and ENSO: a review. *Curr. Clim. Change Rep.* **5**, 296–307 (2019).
34. Zhang, H., Clement, A. & Di Nezio, P. The South Pacific meridional mode: a mechanism for ENSO-like variability. *J. Clim.* **27**, 769–783 (2014).
35. Zhang, H., Deser, C., Clement, A. & Tomas, R. Equatorial signatures of the Pacific Meridional Modes: dependence on mean climate state. *Geophys. Res. Lett.* **41**, 568–574 (2014).
36. Kang et al. Extratropical-Tropical Model Intercomparison Project: protocol and initial results. *Bull. Am. Meteorol. Soc.* **100**, 2589–2605 (2019).
37. Schott, F., McCreary, J. & Johnson, G. in *Earth's Climate* (eds Wang, C. et al.) 261–304 (American Geophysical Union, 2013).
38. Graffino, G., Farnetti, R., Kucharski, F. & Molteni, F. The effect of wind stress anomalies and location in driving Pacific subtropical cells and tropical climate. *J. Clim.* **32**, 1641–1660 (2019).
39. Hwang, Y., Xie, S., Deser, C. & Kang, S. Connecting tropical climate change with Southern Ocean heat uptake. *Geophys. Res. Lett.* **44**, 9449–9457 (2017).
40. Lee, S. Testing of the tropically excited Arctic warming mechanism with traditional El Niño and La Niña. *J. Clim.* **25**, 4015–4022 (2012).
41. Yoo, C., Feldstien, S. & Lee, S. The impact of the Madden-Julian Oscillation trend on the Arctic amplification of surface air temperature during the 1979–2008 boreal winter. *Geophys. Res. Lett.* **38**, L24804 (2011).

Publisher's note Springer Nature remains neutral with regard to jurisdictional claims in published maps and institutional affiliations.

© The Author(s), under exclusive licence to Springer Nature Limited 2020

Methods

SIE. SIE is defined as the total area of the grid boxes in the Arctic or Antarctic that have a sea-ice coverage of 15% or more. For an observational estimate of the seasonal cycle of A and AA SIE, we use the US National Snow and Ice Data Center's Sea Ice Index¹.

WACCM4. To investigate the effect of A and AA sea-ice loss, we performed experiments using the Whole Atmosphere Community Climate Model (WACCM4), a high-top model that participated in CMIP5. WACCM4 has been fully documented by Marsh et al.²⁹. It has a horizontal resolution of 2° latitude by 2.6° longitude, with 66 vertical levels and a model lid that extends up to the lower thermosphere, near 140 km. WACCM4 simulates the climatology of sea ice well in both hemispheres (Extended Data Fig. 1), although AA summer sea-ice cover is more extensive than observations show. In addition to enhanced vertical resolution in the stratosphere and mesosphere, WACCM incorporates an interactive stratospheric chemistry package, and special gravity wave parameterizations for the upper atmosphere. These features give this model a much-improved representation of the stratosphere than low-top models. Employing a high-top model is important, because recent research has identified the stratosphere as a possible pathway for interactions between the polar climate and mid-latitude weather^{14,42,43}. It also allows us to compare these results with previous atmosphere-only experiments using the same model¹². We run WACCM4 coupled with the CICE4 ice model⁴⁴ and the POP2 ocean model⁴⁵.

WACCM experiments with constrained sea-ice conditions. We investigate the effect of AA and A sea-ice loss on the climate system by performing four numerical experiments (outlined in Table 1), each 350 years long, using WACCM: a control run and three perturbed sea-ice runs. The four integrations are as follows: one control run (HIST) with mid-twentieth-century sea-ice conditions in both hemispheres; one run with future sea-ice conditions in the A (FUT-A); one run with future sea-ice conditions in the AA (FUT-AA); and one run with future sea-ice conditions in both the A and AA (FUT-A&AA) (Fig. 1a,b; dashed lines). To obtain the HIST sea-ice conditions, we average six existing WACCM fully coupled historical runs²⁹ over the period 1955–1969 (Fig. 1a,b; solid grey lines); similarly, the FUT ice conditions are obtained by averaging the three existing WACCM fully coupled RCP8.5 runs over the period 2085–2099 (Fig. 1a,b; solid green lines).

We use the ghost flux method outline in Deser et al.²¹ to artificially constrain the seasonal cycle of sea-ice concentration and volume in these integrations to match either HIST or FUT as defined above. The first 100 years of each run are then discarded to focus on the equilibrium response²³. By calculating the difference between the perturbed and control runs, we can isolate the fully coupled equilibrium climate responses to Arctic sea-ice loss (FUT-A minus HIST; denoted A), Antarctic sea-ice loss (FUT-AA minus HIST; denoted AA) and both Arctic and Antarctic sea-ice loss (FUT-A&AA minus HIST; denoted A&AA). For reference, the annual average SIE loss (FUT minus HIST) is 4.3×10^6 km² in the Arctic and 6.6×10^6 km² in the Antarctic (Fig. 1a,b; grey bars). This ratio of A:AA sea-ice loss is typical for CMIP5 models, at least over the historical period (fig. 5 of ref. ⁴⁶).

To achieve the desired seasonal cycle of sea-ice conditions in each hemisphere, we follow the ghost forcing method outlined in the appendix of Deser et al.²¹. This involves specifying a seasonally varying longwave radiative flux to the ice model for each grid box and time step. Ghost forcing refers to the fact that the additional longwave forcing is invisible to other model components, except indirectly through changes in sea ice. This flux is applied only to areas where sea ice is present, but for simplicity does not vary spatially. The longwave radiative flux necessary to replicate the desired sea-ice conditions was calibrated through many iterations of shorter runs. We note that the change in SIE had a linear relationship with additional longwave forcing, except for the summer months, when the relationship was nonlinear; this required us to perform additional iterations before the experimental results lay within an acceptable tolerance of the target values. Figure 1 shows how closely constrained the sea-ice experiments were to their target values from the historical or RCP8.5 integrations. We also note that the 'ghost flux' method used in this study is one of a few techniques commonly used in this type of experiment^{10,22}.

In all of our experiments, all forcings (including ozone-depleting substances that have been suggested to contribute to Arctic amplification⁴⁷) are fixed at 1955 values, except for the added longwave radiative flux used to constrain the sea-ice concentrations. In the same fashion as England et al.¹², we use this period for the control because we are largely focused on the Southern Hemisphere and want to avoid including a perpetual stratospheric ozone hole in the simulations (as the

Antarctic polar stratosphere is severely perturbed at present; see England et al.⁴⁸ for the stratospheric ozone depletion in the WACCM historical runs), but the ozone hole is projected to recover before the end of this century). We have selected periods before and after the existence of the ozone hole so it does not complicate the interpretation of our results. This choice results in a slightly more sea-ice loss than in similar studies, but the results are still broadly comparable because the vast majority of the sea-ice loss is projected to occur in the twenty-first century.

Calculating the atmospheric and oceanic northward heat transport. The oceanic NHT is diagnosed directly from the N_HEAT variable in the ocean history file. The atmospheric net NHT is calculated using the method outlined in the appendix of Kay et al.⁴⁹. This calculation estimates the vertically integrated atmospheric net NHT in equilibrium conditions from the difference between the net top of atmosphere and surface fluxes. The required fields for this calculation are: net longwave and shortwave top of atmosphere radiation, net longwave and shortwave surface radiative fluxes, and net surface sensible and latent heat fluxes (all in W m⁻²).

Data availability

All model output analysed in the study is stored on the data servers at the National Center for Atmospheric Research in Boulder, Colorado, and can be made available upon request from the corresponding author.

Code availability

Where possible, pre-processed variables and the NCL code for reproducing the related figures are publicly available at https://figshare.com/projects/The_Tropical_Responses_to_Projective_Arctic_and_Antarctic_Sea_Ice_Loss/72518. All other code used to produce the figures can be made available upon request from the corresponding author.

References

- Zhang, P. et al. A stratospheric pathway linking a colder Siberia to Barents-Kara Sea sea ice loss. *Sci. Adv.* **4**, eaat6025 (2018).
- De, B. & Wu, Y. Robustness of the stratospheric pathway in linking the Barents-Kara Sea sea ice variability to the mid-latitude circulation in CMIP5 models. *Clim. Dynam.* **53**, 193–207 (2019).
- Holland, M., Bailey, D., Briegleb, B., Light, B. & Hunke, E. Improved sea ice shortwave radiation physics in CCSM4: the impact of melt ponds and aerosols on Arctic sea ice. *J. Clim.* **25**, 1413–1430 (2012).
- Danabasoglu, G. et al. The CCSM4 ocean component. *J. Clim.* **25**, 1361–1389 (2012).
- Rosenblum, E. & Eisenman, I. Sea ice trends in climate models only accurate in runs with biased global warming. *J. Clim.* **30**, 6265–6278 (2017).
- Polvani, L., Previdi, M., England, M., Chiodo, G. & Smith, K. Substantial twentieth-century Arctic warming caused by ozone-depleting substances. *Nat. Clim. Change* **10**, 130–133 (2020).
- England, M., Polvani, L., Smith, K., Landrum, L. & Holland, M. Robust response of the Amundsen Sea Low to stratospheric ozone depletion. *Geophys. Res. Lett.* **43**, 8207–8213 (2016).
- Kay, J. et al. The influence of local feedbacks and northward heat transport on the equilibrium Arctic climate response to increased greenhouse gas forcing. *J. Clim.* **25**, 5433–5450 (2012).

Acknowledgements

M.R.E. is funded by a collaborative agreement between NASA GISS and Columbia University and NSF grants OPP-1643445 and OPP-1744835. L.M.P. is funded by NSF award number 1745029. This material is based on work performed at the National Center for Atmospheric Research, a major facility sponsored by the National Science Foundation. We thank S. Gille, I. Eisenman, S. Sun, M. Mazloff and R. Abernathy for productive discussions.

Author contributions

M.R.E. performed the integrations, carried out the analysis and wrote the first draft of the manuscript. L.M.P. designed the integrations. L.S. provided assistance in setting up the integrations. C.D. designed the study and provided expertise in tropical climate. All authors were heavily involved in interpreting the results and the drafting of the final manuscript.

Competing interests

The authors declare no competing interests.

Additional information

Extended data is available for this paper at <https://doi.org/10.1038/s41561-020-0546-9>.

Correspondence and requests for materials should be addressed to M.R.E.

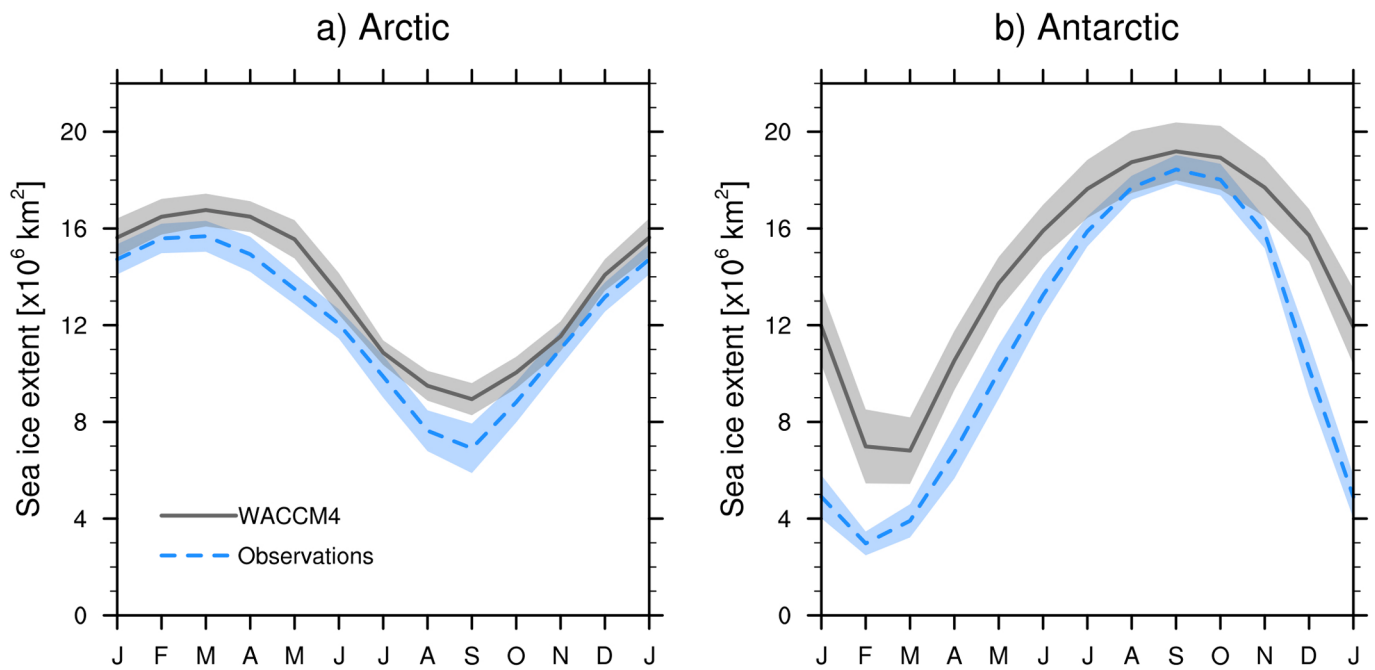
Peer review information Primary Handling Editor: Heike Langenberg.

Reprints and permissions information is available at www.nature.com/reprints.

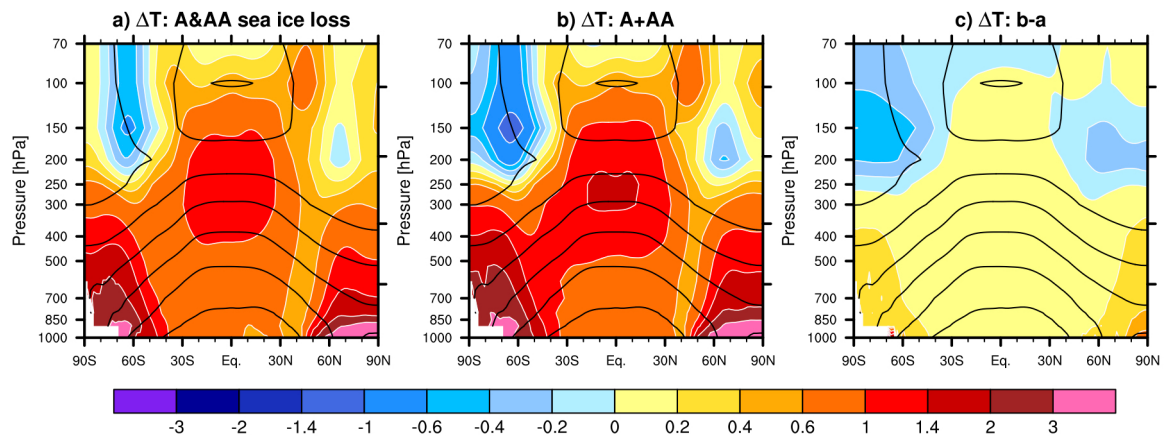
Table 1 | Details of perturbed sea-ice experiments using the fully coupled version of WACCM

Experiment name	Length (yr)	A sea ice	AA sea ice
HIST	350	1955–1969	1955–1969
FUT-A	350	2085–2099	1955–1969
FUT-AA	350	1955–1969	2085–2099
FUT-A&AA	350	2085–2099	2085–2099

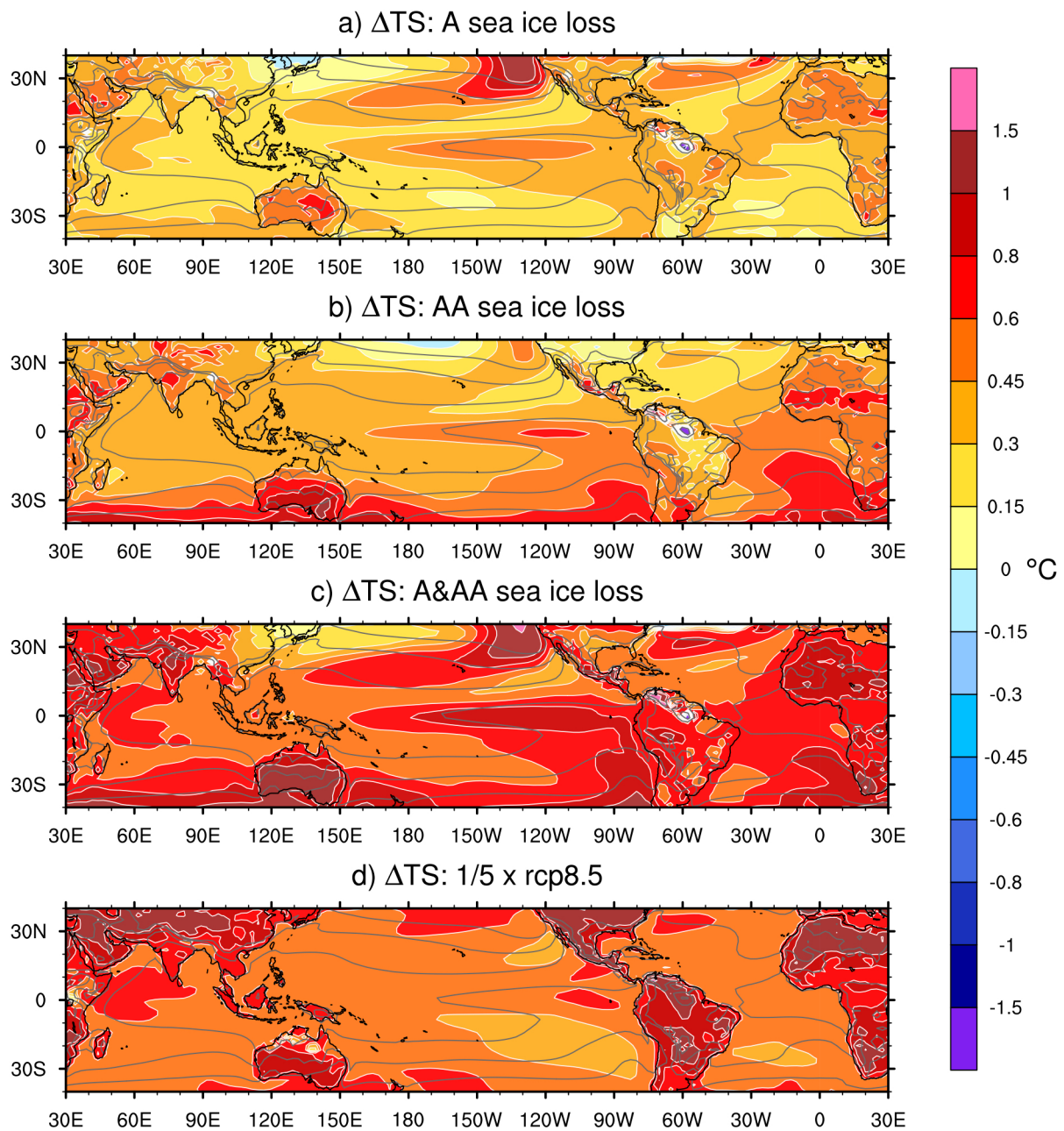
Climatology 1979-2000



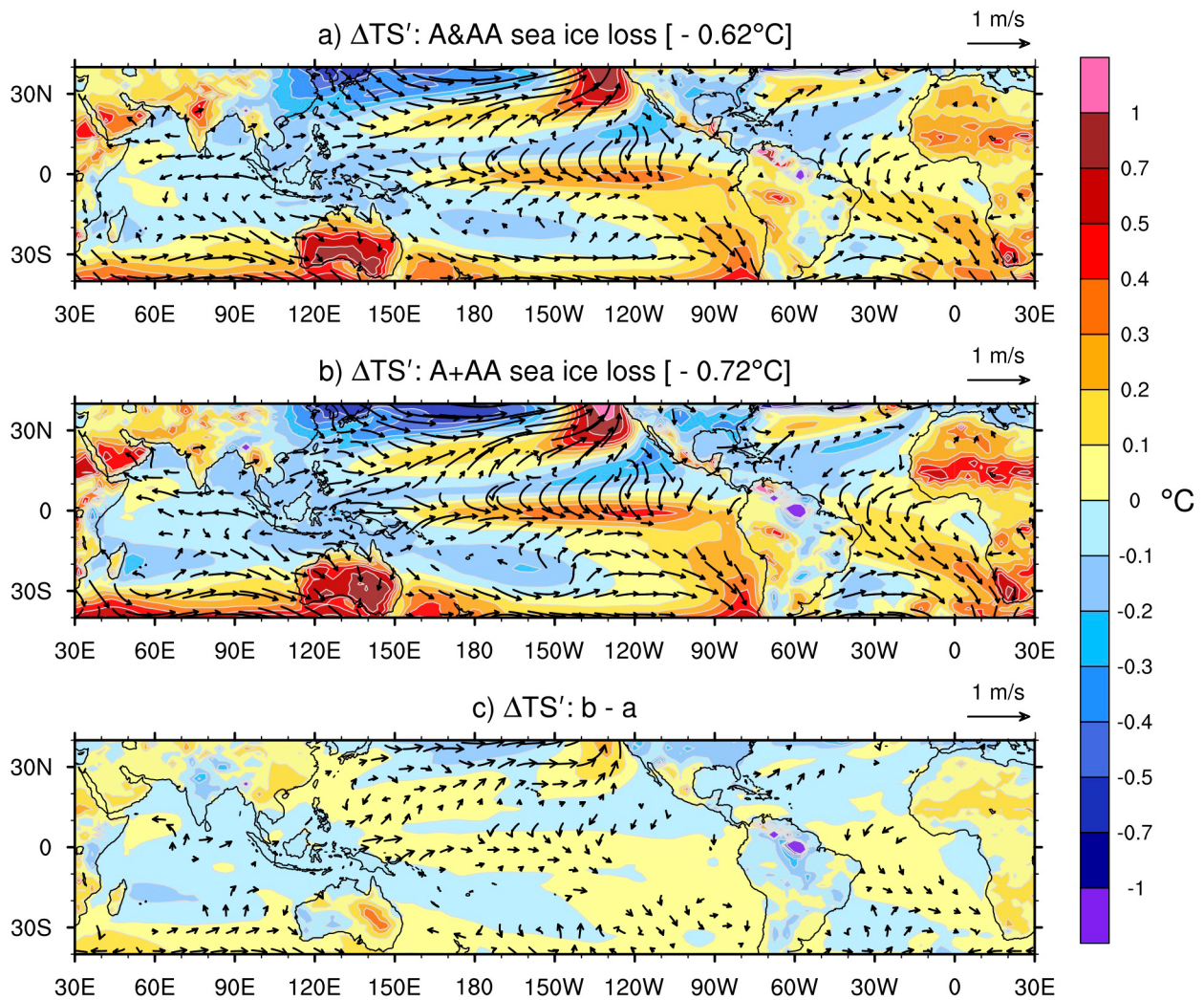
Extended Data Fig. 1 | Arctic and Antarctic sea ice extent climatology. The seasonal cycle of (a) Arctic and (b) Antarctic SIE [10^6 km^2] averaged over the years 1979–2000 from six WACCM historical runs (grey) and observational data from the NSIDC Sea Ice database (NSIDC, 2019) (blue). The shading shows the $\pm 2\sigma$ envelope.



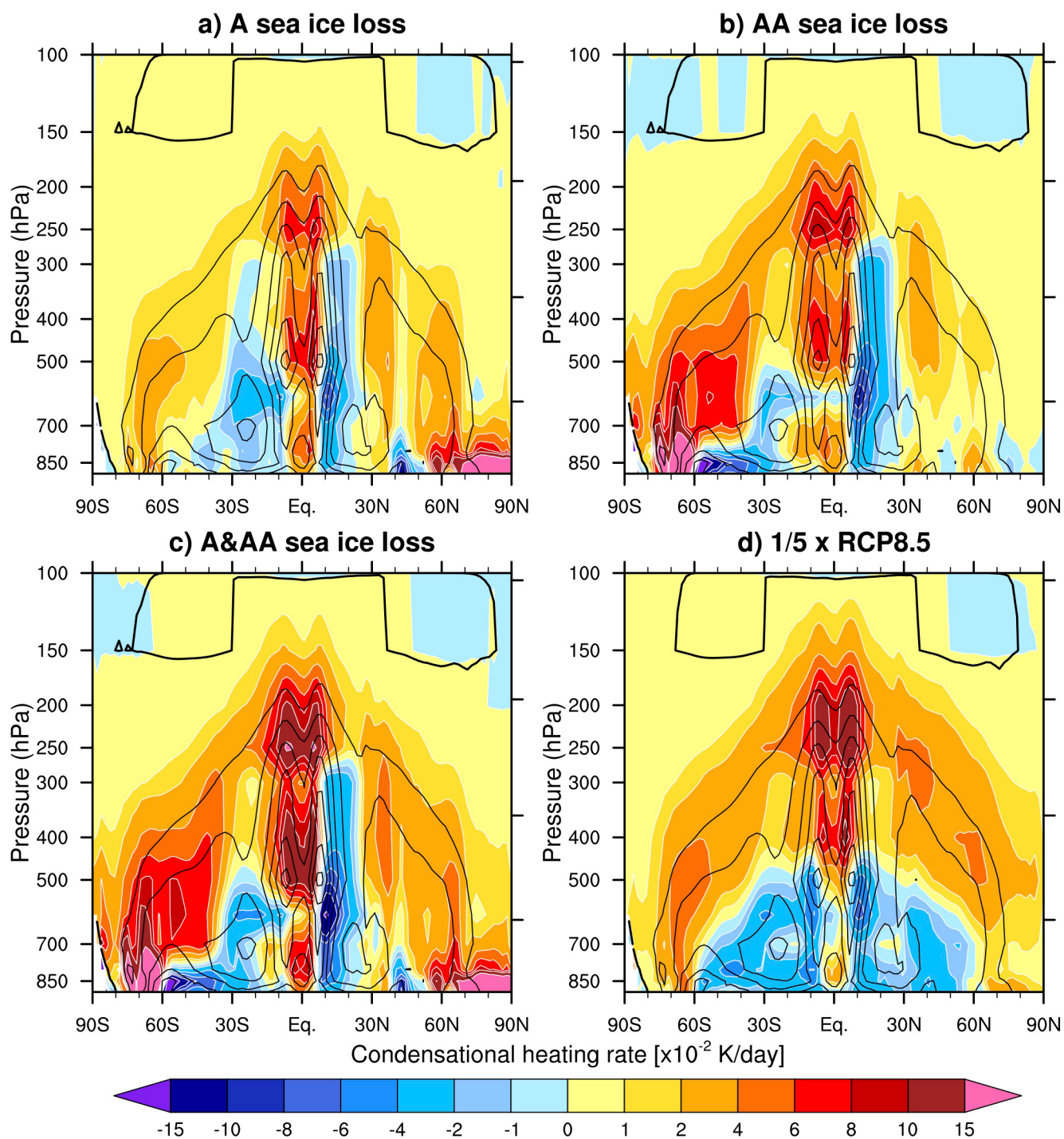
Extended Data Fig. 2 | Additivity of the zonally average temperature response to sea ice loss. (a) The zonally averaged temperature response [$^{\circ}\text{C}$] to both Arctic and Antarctic sea ice loss as a function of latitude and height. (b) The linear sum of the response to Arctic sea ice loss and the response to Antarctic sea ice loss. (c) The difference between panels a, b. Contours show the climatological temperature structure with intervals of 15°C .



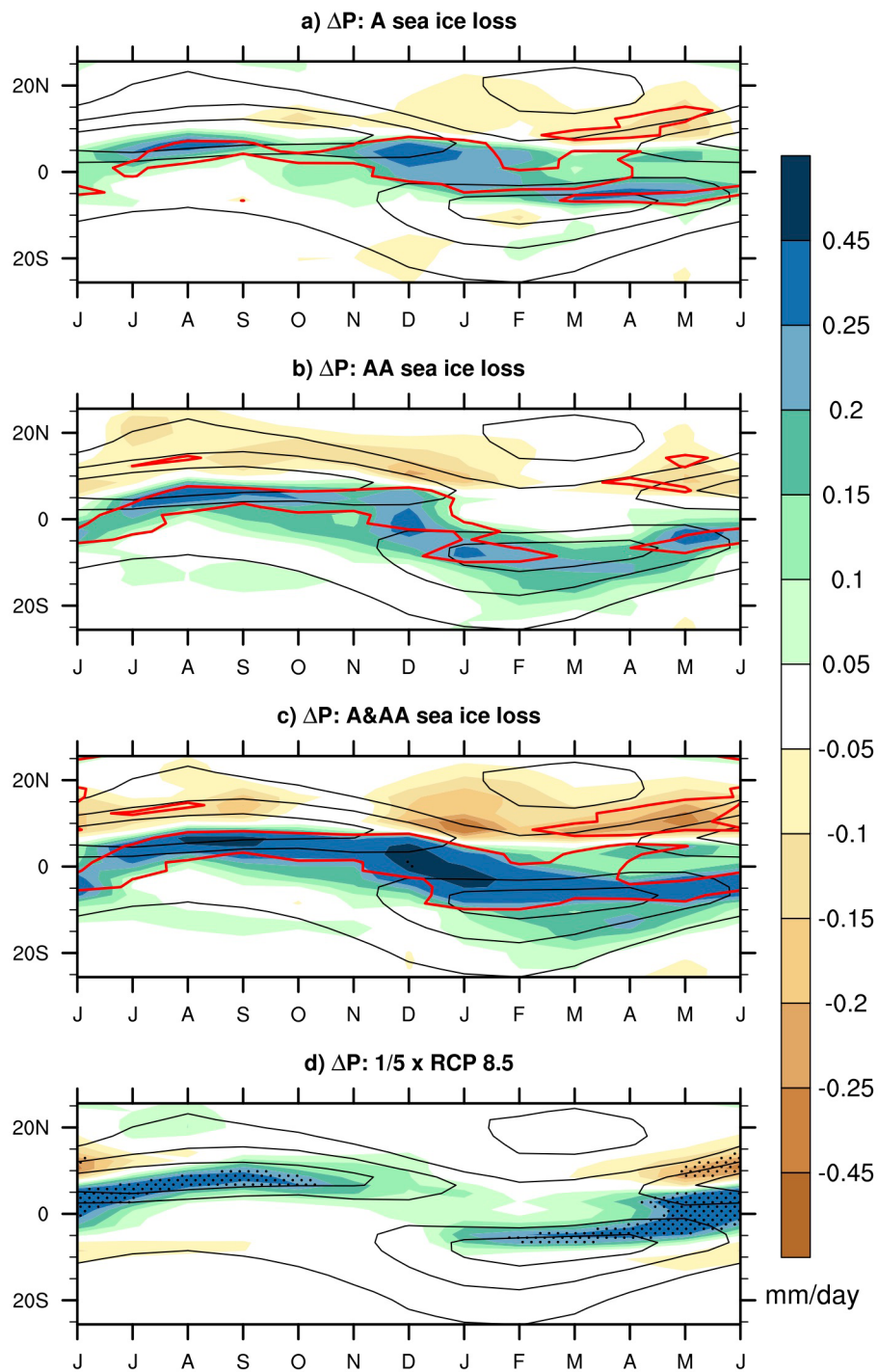
Extended Data Fig. 3 | Tropical surface temperature response to sea ice loss. (Shading) The annual mean surface temperature response [$^{\circ}$ C] to (a) Arctic sea ice loss, (b) Antarctic sea ice loss and (c) both Arctic and Antarctic sea ice loss compared to (d) the projected changes under RCP8.5, the 15-year average of 2085-2099 minus the 15-year average of 1955-1969, (scaled by a factor of 1/5). The contours show the climatological surface temperature with contour intervals of 4 $^{\circ}$ C.



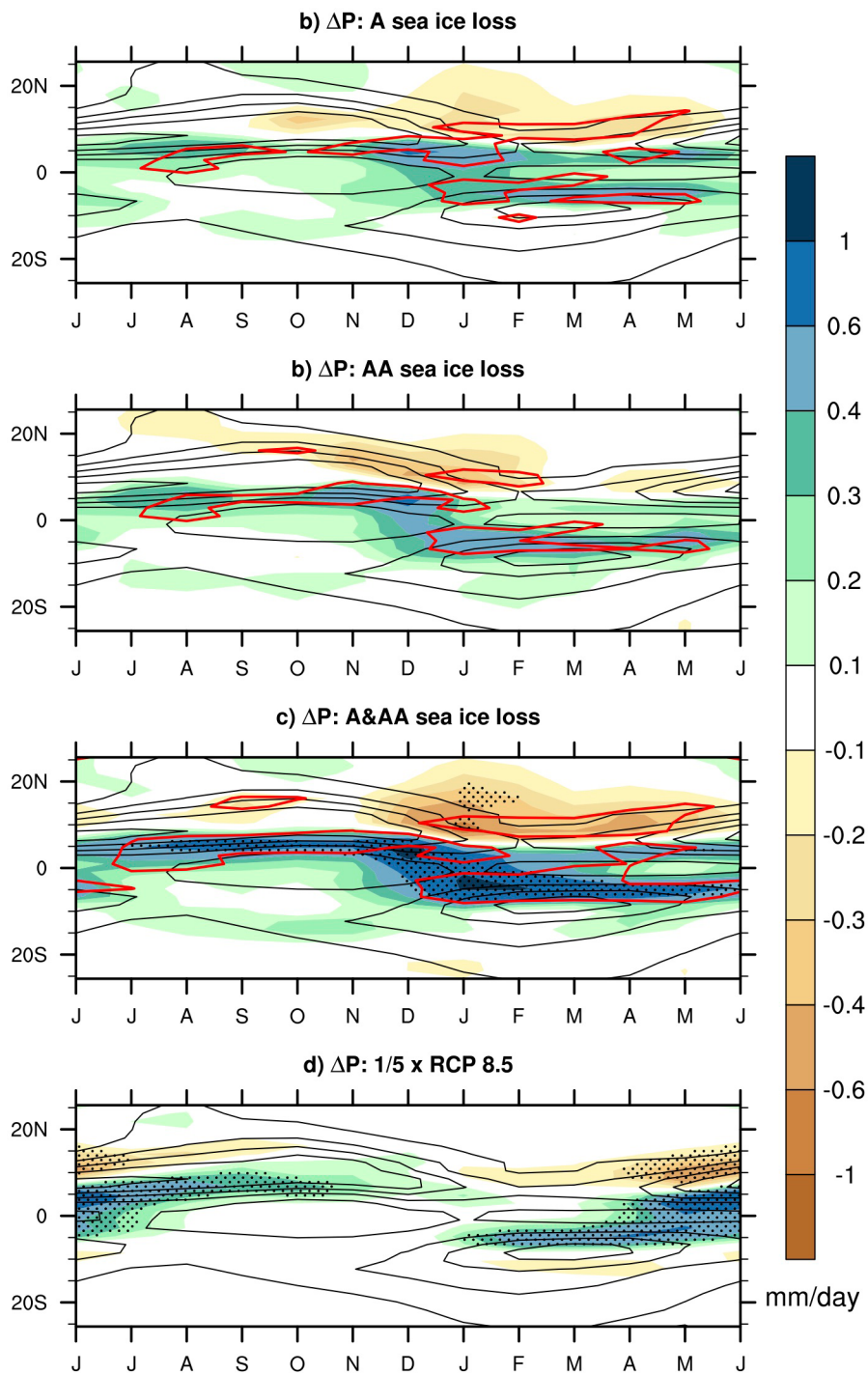
Extended Data Fig. 4 | Additivity of the surface temperature response to sea ice loss. (a) The surface temperature response [°C] after subtracting the mean tropical SST warming (shaded contours) and the surface wind response [m/s] (vectors) to combined Arctic and Antarctic sea ice loss. (b) As in panel (a) except for the linear sum of the response to Arctic sea ice loss and the response to Antarctic sea ice loss. (c) The difference between panels a and b.



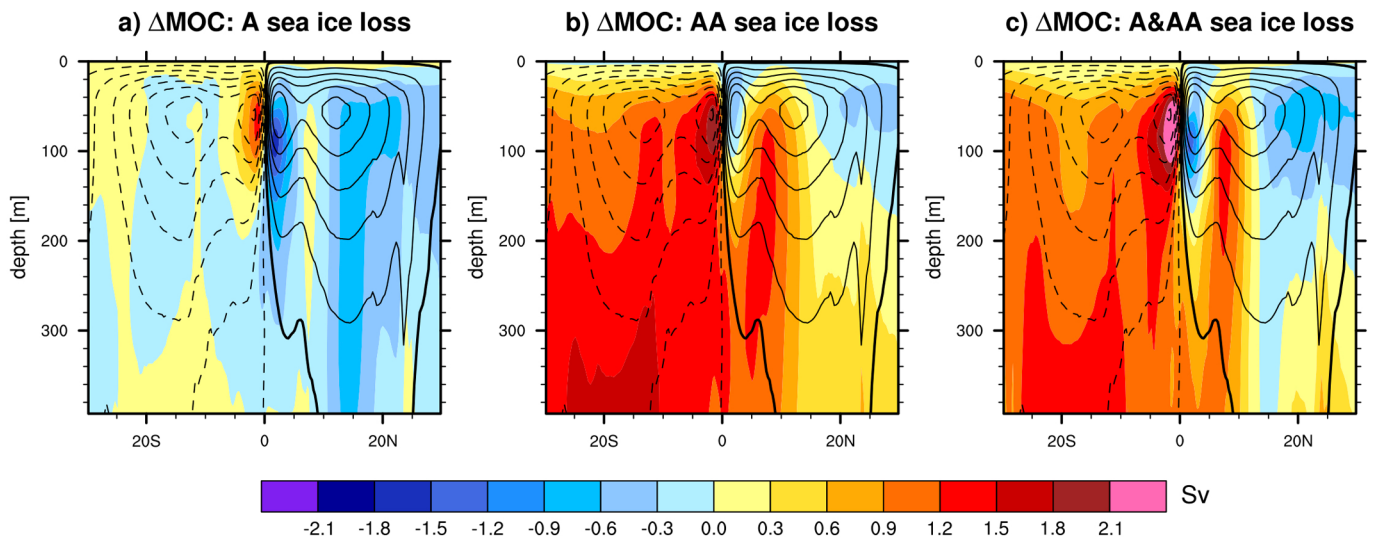
Extended Data Fig. 5 | The condensational heating rate response to sea ice loss. The response of annual mean condensational heating rate [$\times 10^{-2}$ °C/day] to (a) Arctic sea ice loss, (b) Antarctic sea ice loss and (c) both Arctic and Antarctic sea ice loss. (d) The projected change in annual mean condensational heating rate under RCP8.5, the 15-year average of 2085-2099 minus the 15-year average of 1955-1969. Note that the response in panel (d) is scaled by a factor of 1/5.



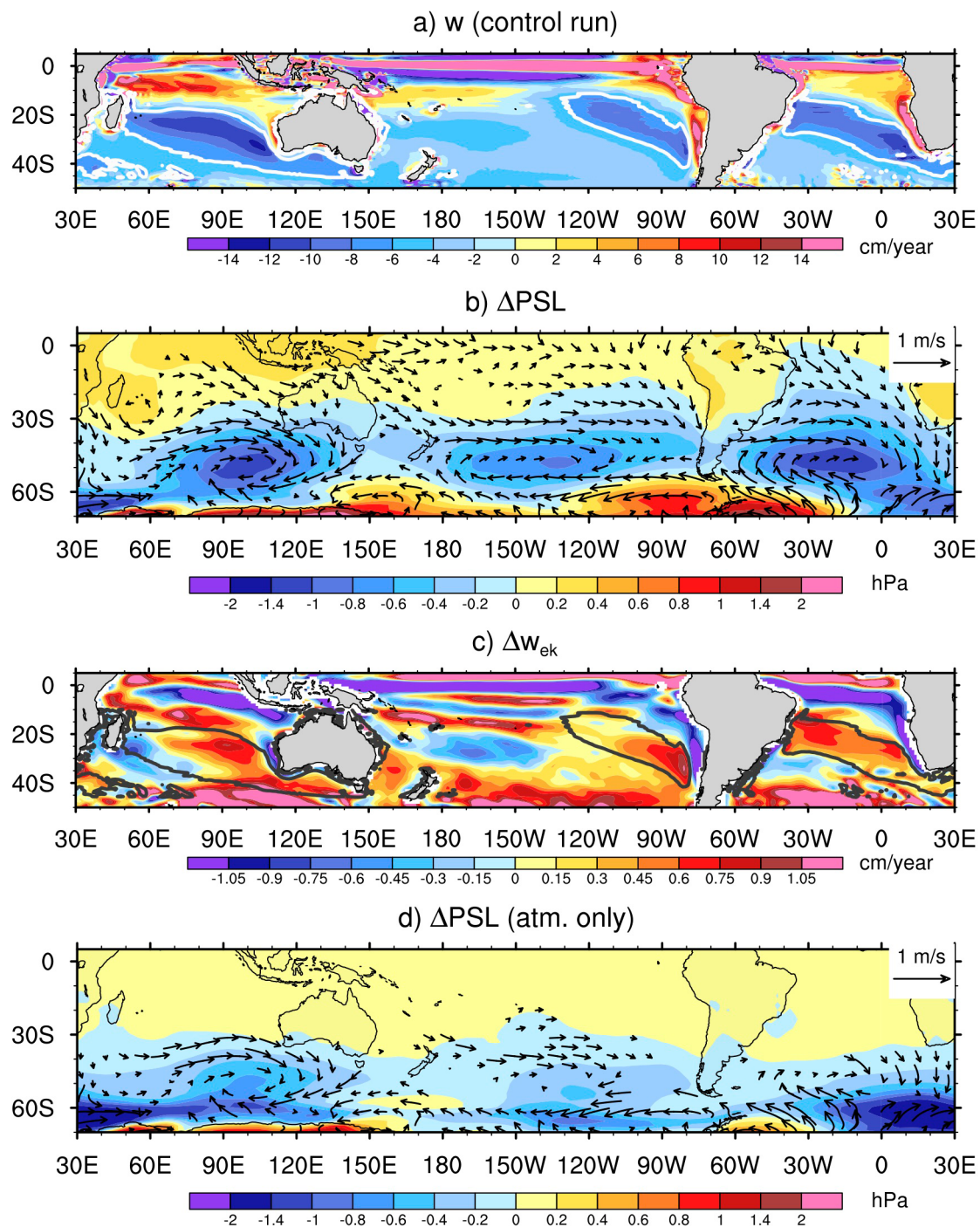
Extended Data Fig. 6 | Zonally averaged precipitation response to sea ice loss. (Shading) The response of the zonally averaged precipitation [mm/day] to (a) Arctic sea ice loss, (b) Antarctic sea ice loss and (c) both Arctic and Antarctic sea ice loss. (d) The projected change under RCP8.5, the 15-year average of 2085-2099 minus the 15-year average of 1955-1969. Note that the response in panel (d) is scaled by a factor of 1/5. Stippling shows a statistically significant response at 95% confidence. (Contours, black) The zonally averaged precipitation with contour intervals of 2 mm/day. Regions are highlighted (contours, red) in which the response is over 20% of the RCP8.5 response.



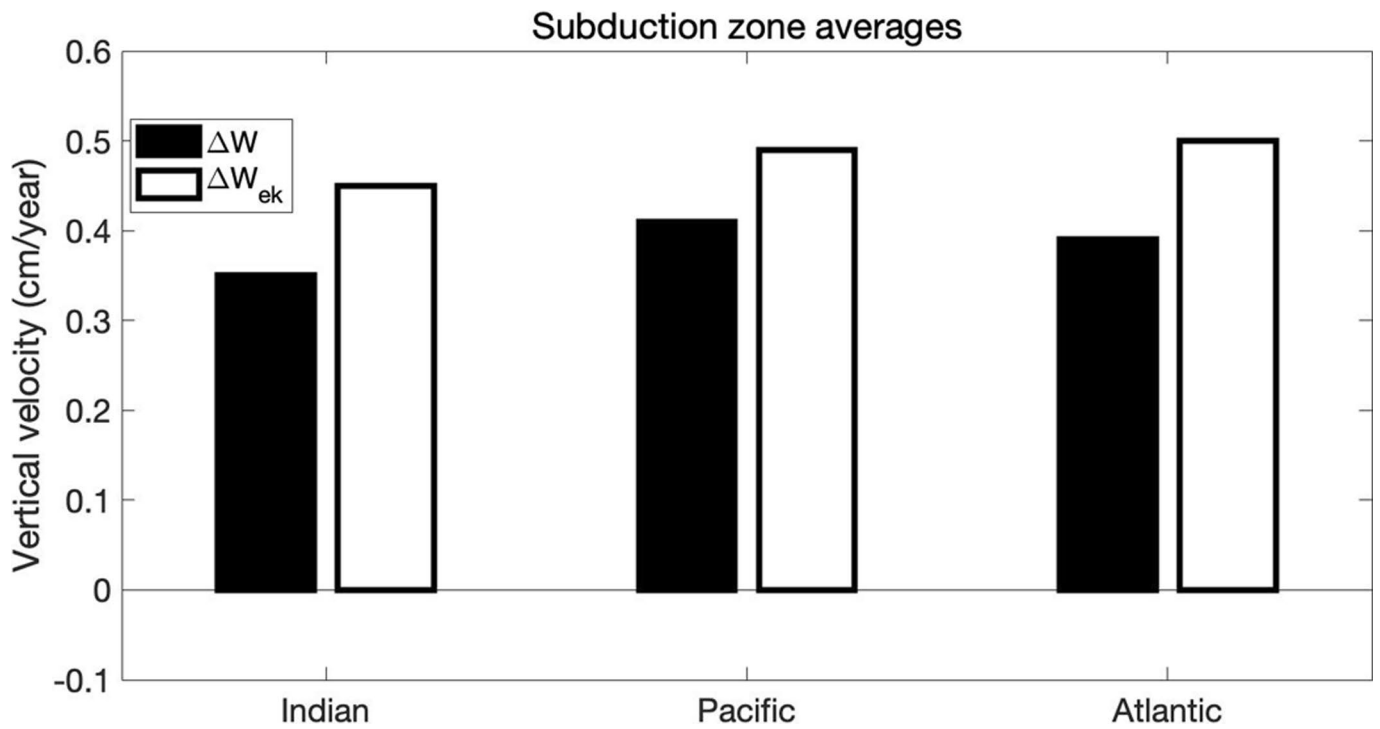
Extended Data Fig. 7 | Zonally averaged (Pacific sector) precipitation response to sea ice loss. As in Extended Data Fig. 6 but for the Pacific sector (130°E-100°W).



Extended Data Fig. 8 | The response of the Pacific subtropical meridional overturning circulation to sea ice loss. (Shading) The depth-latitude response of the Pacific subtropical meridional overturning circulation [Sv] to (a) Arctic sea ice loss, (b) Antarctic sea ice loss and (c) both Arctic and Antarctic sea ice loss. (Contours) The climatological meridional overturning circulation with contour intervals of 5 Sv. The solid lines indicate positive values (clockwise flow), the dashed lines indicate negative values (anti-clockwise flow) and the thick black contour indicates the 0 Sv contour.



Extended Data Fig. 9 | Connecting the slowdown of the subtropical meridional overturning circulation to Antarctic sea ice loss. (a) Average vertical velocity in the upper-100m of the ocean in the control run. The white contours enclose the subduction zones, which we define to be $< -6\text{ cm/year}$. (b) The response of mean sea level pressure [hPa] (shaded) and surface wind [m/s] (vectors) to Antarctic sea ice loss. (c) The response of the vertical Ekman velocity to Antarctic sea ice loss. Positive values indicate anomalous upwelling (Ekman suction) and negative values indicate anomalous downwelling (Ekman pumping). As in panel (a) the black contours enclose the subduction zones. (d) Same as panel (b) but for the atmosphere-only experiments.



Extended Data Fig. 10 | Vertical velocities in the subduction zones. Averaged over the three subduction zones (the Indian, Pacific and Atlantic; as shown in Extended Data Fig. 9a), the response of the vertical velocity in the upper-100m to Antarctic sea ice loss (black bars) and the response of the vertical Ekman velocity (white bars) [cm/year].